Theoretical Chemistry Accounts (2021) 140:1
https://doi.org/10.1007/s00214-020-02703-y

REGULAR ARTICLE

Insights into the mechanism and regioselectivity of the [3 + 2] cycloaddition reactions of cyclic nitrone to nitrile functions with a molecular electron density theory perspective

Haydar A. Mohammad-Salim[1] · **Nivedita Acharjee**[2] · **Hassan H. Abdallah**[3]

Received: 13 September 2020 / Accepted: 30 November 2020 / Published online: 3 January 2021

Abstract
A molecular electron density theory study is presented for [3 + 2] cycloaddition (32CA) reactions of 2,2-dimethyl-1-pyrroline-1-oxide with the nitrile functions to analyse the mechanism and experimentally observed regioselectivity. Electron localisation function (ELF) study predicts zwitter-ionic character of the cyclic nitrone, allowing its participation in *zw*-type 32CA reactions associated with high energy barrier demanding overcome through appropriate electrophilic–nucleophilic interactions. Analysis of the CDFT indices predict the global electronic flux from the strong nucleophilic nitrone to the electrophilic nitrile functions. These 32CA reactions are endergonic with reactions Gibbs free energies between 5.5 and 39.2 kcal·mol^{-1} in toluene. The *ortho* regiochemical pathway is preferred owing to the higher thermodynamic stability of the 2,3-dihydro-1,2,4-oxadiazole derivatives. The 32CA reaction of the nitrile function with carbomethoxy substituent is more facile relative to that with the phenyl substituent. Bonding evolution theory study predicts *one-step* mechanism with early TSs for the *ortho* pathway, while a *one-step-two-stage* mechanism is predicted for the *meta* reaction path, in conformity with the ELF and AIM topological studies at the TSs.

Keywords Molecular electron density theory · Nitriles · [3 + 2] cycloaddition reactions · Electron localisation function

1 Introduction

The nitrile (C≡N) function represents an excellent candidate for [3 + 2] cycloaddition (32CA) reactions to open up useful synthetic pathways for several heteroaromatic compounds. However, the limited applicability of nitriles in 32CA reactions is attributed to their lower reactivity in these reactions relative to other triple bonded reacting functions [1–4]. Nitriles demand a strong electron acceptor substituent to react with acyclic nitrones, while methyl cyanide remains inert to such 32CA reactions even under drastic conditions [1–3]. Hermkens and coworkers performed detailed experimental studies to outline the scope of nitrone-nitrile 32CA reactions, while Eguchi et al. designed the remarkable reactivity of acetonitrile with 4-azahomoadamant-4-ene-*N*–oxide and cyclic nitrones leading to 2,3-dihydro-1,2,4-oxadiazole derivatives (Scheme 1) [2, 5–7].

Since the last two decades, computational chemistry has emerged as an important tool to analyse the experimentally observed reactivity and selectivity outcomes by developing a systematic outline of the mechanism of chemical reactions [8]. However, in spite of the ever-increasing modern applications of the computational science in chemistry, the underlying theories of organic chemistry had not experienced major breakthrough since last 40 years, until in 2016 Domingo proposed the molecular electron density theory (MEDT) to recognise the decisive role of electron density changes in the molecular reactivity [9, 10]. Since last 4 years, MEDT has successfully analysed the experimental outcome of several 32CA reactions [10–12]. Recently, we have applied the MEDT concept to analyse

Supplementry information The online version of this article (https://doi.org/10.1007/s00214-020-02703-y) contains supplementary material, which is available to authorized users.

✉ Haydar A. Mohammad-Salim
hayder.salim@uoz.edu.krd

[1] Department of Chemistry, University of Zakho, Duhok 42001, Iraq

[2] Department of Chemistry, Durgapur Government College, Durgapur, West Bengal 713214, India

[3] Department of Chemistry, Salahaddin University-Erbil, Erbil 44001, Iraq

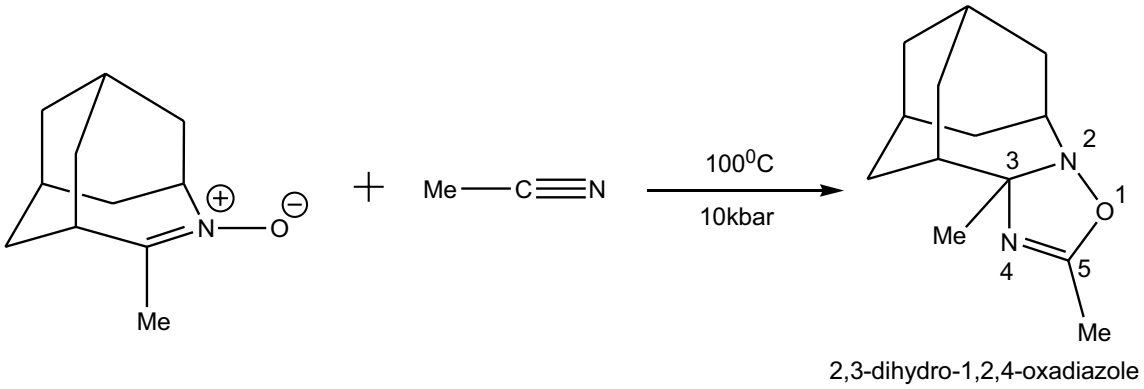

Scheme 1 32CA reaction of 4-azahomoadamant-4-ene-*N*-oxide with acetonitrile

the experimental outcome of strain promoted and catalysed 32CA reactions and the observed chemo-, regio- and stereoselectivite synthesis of spiroisoxazolines [13–17].

Within the MEDT framework, the three atom components (TACs) participating in the 32CA reactions are classified by characterising their electronic structure, into *pseudodiradical*, *pseudo*(mono)*radical*, carbenoid and zwitter-ionic type, which enables their respective participation in *pdr*- type, *pmr*-type, *cb*-type and *zw*-type 32CA reactions [10, 11]. These 32CA reactions show different reactivity profiles; the *pdr*-type 32CA reactions are associated with lower energy barrier and take place easily, while the *zw*-type 32CA reactions show high energy barrier, demanding overcome through electrophilic–nucleophilic interaction between the reactants [16].

The 32CA reactions of acyclic nitrones with the nitrile function were theoretically studied by Wagner et al. and Kuznetsov et al. in 2003 [18, 19]. However, neither of these studies have addressed the mechanistic differences in the feasible reaction paths and the role of electron density flux on the substituent effects of nitrone-nitrile 32CA reactions.

Herein, we present an MEDT study at the B3LYP/6-311 ++G(d,p) level for 32CA reactions of a cyclic nitrone, 2,2-dimethyl-1-pyrroline-1-oxide **1** with nitriles **2** and **3** bearing carbomethoxy and phenyl substituents, experimentally realised by Eguchi and coworkers (see Scheme 2) [5]. These 32CA reactions are completely regioselective leading to 2,3-dihydro-1,2,4-oxadiazole derivatives.

We have presented this MEDT study in six Sects. 3.1–3.6 (1); in Sect. 3.1, the topological analysis of the electron localisation function (ELF) at the ground state structures of the reagents **1**–**3** is performed to represent their electronic structure and consequently to assess their reactivity in 32CA reactions [20, 21]. (2) in Sect. 3.2, reactivity indices defined within the conceptual density functional theory (CDFT) are analysed to comprehend the polarity of the 32CA reactions [22, 23]. (3) in Sect. 3.3, potential energy surfaces (PES) [24] along the feasible regioisomeric channels of the 32CA reactions are studied to predict the energy profiles and the global electron density transfer (GEDT) is calculated at the TSs [25]. (4) in Sect. 3.4, the conjunction of ELF with Thom's catastrophe, namely the bonding evolution theory (BET)

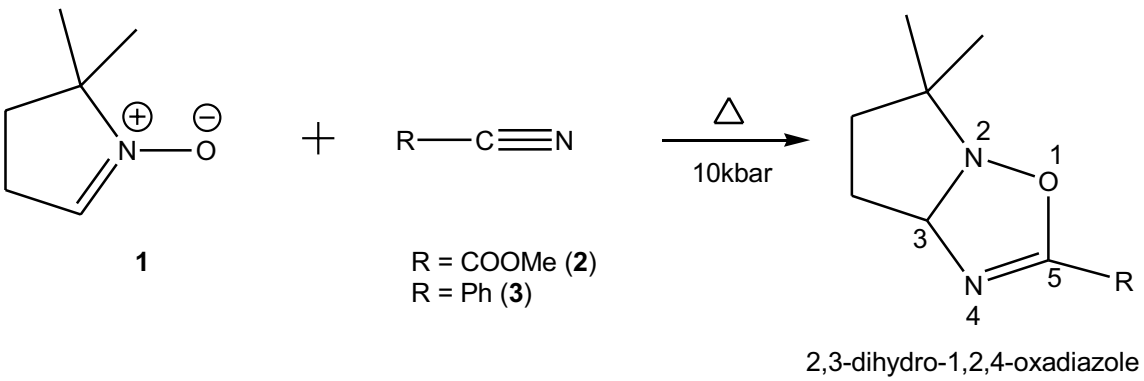

Scheme 2 32CA reaction of 2,2-dimethyl-1-pyrroline-1-oxide (**1**) with nitriles **2** and **3**

proposed by Krokidis, is used to structure the mechanism and determine the energy cost (EC) for electron density changes along the regioisomeric paths [20, 21, 26, 27]. (5) in Sect. 3.5, the ELF of the located TSs is analysed; (6) in Sect. 3.6, the nature of interatomic interactions at the reacting centres of the TSs is analysed by the topological analysis of the AIM proposed by Bader et al. [28, 29].

2 Computational methods

The Berny analytical gradient optimisation method was employed at the B3LYP/6-311 ++G(d,p) level for the optimisation of the stationary points along the potential energy surface of the 32CA reactions [30, 31]. The use of B3LYP functional has been justified as a reliable and accurate method in the analysis of several recent 32CA reactions [32–35].

Frequency calculations at the optimised TSs confirmed the presence of one imaginary frequency, while the absence of imaginary frequency was verified for the local minimum. Intrinsic Reaction coordinate (IRC) calculations using Gonzales–Schlegal integration method were carried out to verify the minimum energy reaction pathway connecting the reactants and products via the located TSs [36–38].

Solvent effects in toluene were considered using polarizable continuum model (PCM) by modelling the solvent using self-consistent reaction field (SCRF) method [39–43].

The CDFT indices are calculated using equation reviewed in Reference 23 [22, 23]. The global electron density theory (GEDT) at the TSs of each reacting framework was calculated from natural population analysis (NPA) as follows [25, 44, 45]:

$$\text{GEDT (f)} = \sum_{q \in f} q$$

where q represents the atomic charges, the summation of charges on all atoms in the considered framework represents the GEDT, the positive sign of GEDT indicating global electronic flux from that framework to the other.

Topological analysis of the ELF at the reagents [20, 21], TSs and IRC points and calculation of Quantum Theory of Atoms-in Molecules (QTAIM) parameters [28, 29] are calculated using Multiwfn software [46] and the isosurfaces are visualised using UCSF Chimera software [47]. Gaussian 16 package has been used for all calculations [48].

3 Results and discussion

3.1 ELF topological analysis of nitrone 1, and nitriles 2 and 3

In 1990, Becke and Edgecombe constructed the ELF concept, which was illustrated in 1994 by Silvi and Savin to propose a quantitative connection between the electron density distribution and the chemical structure of molecules [20, 21]. Under the MEDT framework, a reasonably good correlation has been established between the electronic structure of three atom components (TACs) and their reactivity in 32CA reactions [9–11].

Herein, the ELF of the ground state structures of the reagents **1**–**3** is studied to represent their electronic structures and reactivity in 32CA reactions. Table 1 lists the significant ELF valence basin populations of nitrone **1** and the nitriles **2** and **3**, while the ELF localisation domains are shown in Fig. 1. Based on the ELF valence populations, the Lewis structures of the reagents are proposed and are given in Fig. 2.

The ELF of nitrone **1** shows two monosynaptic basins, V(O1) and V'(O1) integrating 5.91 e, one disynaptic basin V(C3,N2) integrating 3.84 e and one disynaptic basin V(N2,O1) integrating 1.41 e, which are associated with the non-bonding electron density on O1 oxygen, underpopulated C3–N2 double bond and underpopulated N2–O1 single bond, respectively.

The ELF of nitriles **2** and **3** shows one monosynaptic basin V(N4) integrating 3.13 e (**2**) and 3.22 e (**3**), associated with non-bonding electron density on N4 nitrogen atom and disynaptic basins for the C5–N4 bonding region with total integrating populations of 4.50 e (**2**) and 4.40 e (**3**), associated with the underpopulated C5–N4 triple bond.

After establishing the bonding pattern of the reagents, the atomic charge distribution of nitrone **1** and nitriles **2** and **3** was analysed through NPA (Fig. 2) [44, 45]. O1 oxygen atom of nitrone **1** is negatively charged (−0.541 e). C3

Table 1 B3LYP/6-311 ++G(d,p) calculated most significant ELF valence basin populations at **1-3.** ELF valence basin populations are given in average number of electrons, e

	1	2	3
V(O1)	3.02		
V'(O1)	2.89		
V(C3,N2)	3.84		
V(N2,O1)	1.41		
V(N4)		3.13	3.22
V(C5,N4)		1.87	2.20
V'(C5,N4)		0.17	2.20
V''(C5,N4)		2.29	
V'''(C5,N4)		0.17	
V(C5,C6)		2.35	2.35

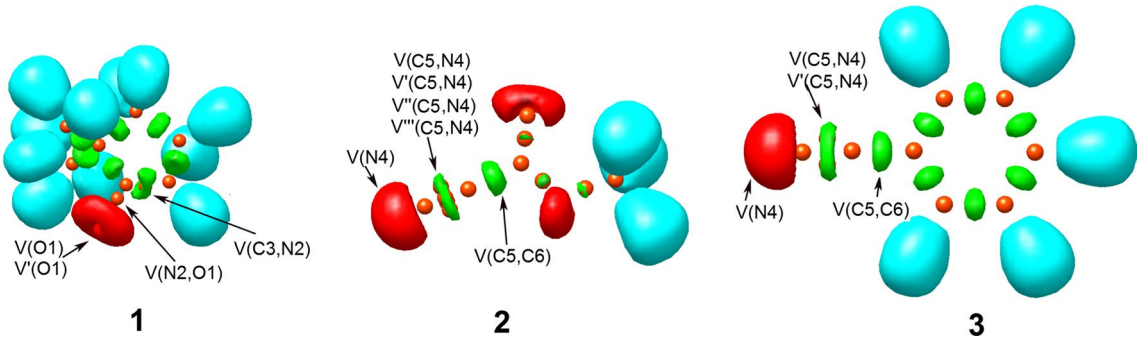

Fig. 1 B3LYP/6-311++G(d,p) ELF localisation domains represented at an isosurface value of ELF = 0.83 of nitrone **1** and nitriles **2** and **3.** Blue colour represents the protonated basins, green coloured ones are the disynaptic basins, and red colour is used to represent the monosynaptic basins. The attractor positions are represented as orange spheres

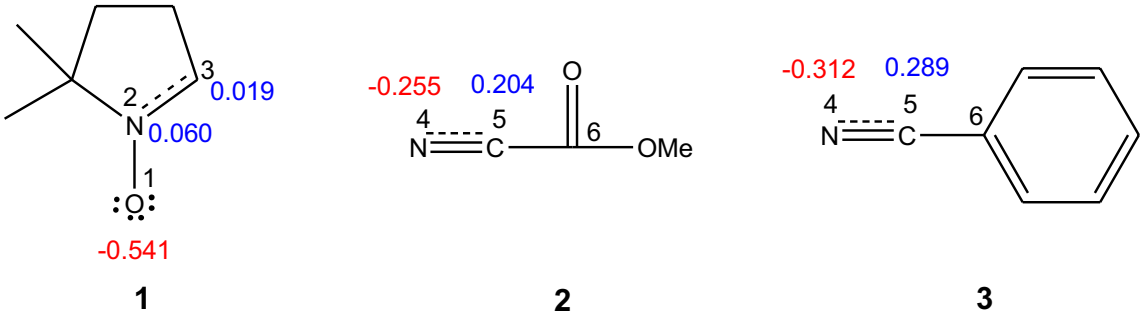

Fig. 2 B3LYP/6-311++G(d,p) calculated natural atomic charges, in average number of electrons e, of nitrone **1** and nitriles **2** and **3**. Negative charges are coloured in red, and positive charges in blue

carbon shows charge of 0.019 e, while N2 nitrogen is positively charged (0.060 e).

This suggests charge separation in the nitrone although differing from the charges expected by the Lewis's bonding model. Although nitrone **1** is classified as a "zwitterionic" TAC from ELF study, this terminology is not synonymous to the dipolar electronic structure of the nitrones. Instead, it indicates the specific bonding pattern (considering no charges) of the resonance Lewis structure represented by Huisgen for "1,3-dipoles" [49].

In the nitriles **2** and **3**, nitrogen N4 shows negative charge values −0.255 (**2**) and −0.312 (**3**), while C4 bearing positive charge 0.204 (**2**) and 0.289 (**3**), indicating the influence of electronically biased carbomethoxy (**2**) and phenyl (**3**) substituents of the nitrile functions.

3.2 Analysis of the CDFT indices of nitrone 1, and nitriles 2 and 3

The concept of "*Conceptual DFT*", originated from the pioneering work of Parr, has been utilised in several studies to assess the chemical reactivity of structures participating in 32CA reactions [22, 23, 50–53]. Reactivity indices defined within the conceptual DFT, namely the CDFT indices, have well documented literature and provide an initial comprehension of the molecular reactivity by addressing the chemical behaviour of the reactants [23]. Domingo defined the standard scales for electrophilicity and nucleophilicity indices at the B3LYP/6-31G(d) level, which has therefore been employed herein for the CDFT analysis [54, 55]. Consequently, the CDFT indices, electronic chemical potential, μ, chemical hardness, η, electrophilicity, ω, and nucleophilicity, *N*, at the ground state of nitrone **1**, and nitriles **2** and **3**, are listed in Table 2 [56–59].

Table 2 B3LYP/6-31G(d) CDFT indices of nitrone **1** and nitriles **2** and **3.** μ, η, ω and *N* represent electronic chemical potential, chemical hardness, electrophilicity and nucleophilicity indices, respectively, and are expressed in eV

	μ	η	ω	*N*
1	− 2.83	5.50	0.73	3.54
2	− 5.36	6.69	2.15	0.41
3	− 4.31	5.85	1.59	1.88

The electronic chemical potentials μ of nitrone **1**, $\mu = -2.83$ eV (**1**) are higher than that of nitriles **2** ($\mu = -5.36$ eV) and **3** ($\mu = -4.31$ eV), suggesting that

along the 32CA reaction, the electron density will flux from nitrone **1** to the nitriles **2** and **3** [23, 56].

The electrophilicity ω index and the nucleophilicity N index of nitrone **1** is 0.73 and 3.54 eV, respectively, being classified as a weak electrophile and a strong nucleophile on the respective scales [54, 55, 58, 59]. The nitriles **2** and **3,** with electrophilicity indices $\omega = 2.15$ eV (**2**) and $\omega = 1.59$ eV (**3**) are classified as strong electrophiles and with nucleophilicity indices $N = 0.41$ eV (**2**) and $N = 1.88$ eV (**3**) as weak nucleophiles. Note that the replacement of the carbomethoxy substituent in **2** by phenyl in **3**, decreases the electrophilicity of the nitrile, suggesting a more feasible electrophilic–nucleophilic interaction in the 32CA reaction between **1** and **2**, relative to that between **1** and **3**. Consequently, along these *zw*-type 32CA reactions the nitriles **2** and **3** will behave as electrophiles, while nitrone **1** will behave as a nucleophile, in conformity with the electronic chemical potentials μ of these species.

3.3 Analysis of the energy profile associated with the 32CA reactions of nitrone 1 with nitriles 2 and 3

Due to non-symmetry of the nitrile functional, two regioisomeric paths, namely the *ortho* and *meta* (see Scheme 3), are feasible for these 32CA reactions. The *ortho* reaction path is associated with the formation of O1–C5 and C3–N4 bonds, while the *meta* channel with the formation of O1–N4 and C3–C5 bonds. The stationary points along these two reactions paths were located and characterised, the reagents, nitrone **1**, nitriles **2** and **3**, two TSs for each 32CA reaction, **TS1**, **TS2**, **TS3** and **TS4** and the corresponding adducts **4**–**7**, respectively, for the 32CA reactions of nitrone **1** with **2** and **3**. **TS1** and **TS3** correspond to the *ortho* TSs leading to 2,3-dihydro-1,2-4-oxadiazoles **4** and **6**, while **TS2** and **TS4** are the *meta* TSs leading to 2,3-dihydro-1,2-5-oxadiazoles **5** and **7**, respectively. The relative Gibbs free energies at the stationary points are given in Scheme 4, while the relative energy, enthalpy and entropies are given in Table S3 of the Supplementary Information. The absolute energy, enthalpy, free energy and entropies of the stationary states are given in Table S1 and Table S2 of the Supplementary Information.

The energy profile of the 32CA reactions was studied to arrive at some important conclusions (1) These 32CA reactions show positive reaction Gibbs free energies, ΔG of 3.4 (**4**), 29.0 (**5**), 6.1 (**6**) and 36.3 (**7**) in gas phase and 5.5 (**4**), 31.0 (**5**), 9.4 (**6**) and 39.2 (**7**) in toluene, suggesting endergonic reaction, demanding the analysis of the thermodynamic stability of the cycloadducts to predict the preferred regiochemical path. Along the *ortho* channel, the reaction enthalpies are -10.5 (**4**) and -8.5 (**6**) kcal·mol^{-1} in gas phase and -8.6 (**4**) and 5.0 (**6**) kcal·mol^{-1} in toluene, while along the *meta* reaction path, the products show positive reaction enthalpies 14.7 (**5**) and 21.9 (**7**) kcal·mol^{-1} in gas phase and 16.7 (**5**) and 24.9 (**7**) kcal·mol^{-1} in toluene. Thus, the *ortho* adducts show higher relative stability than the *meta* ones owing to their negative reaction enthalpies and lower reaction free energies, suggesting preference for the *ortho* reaction path leading to 2,3-dihydro-1,2,4-oxadiazoles, in complete agreement with the experimental studies

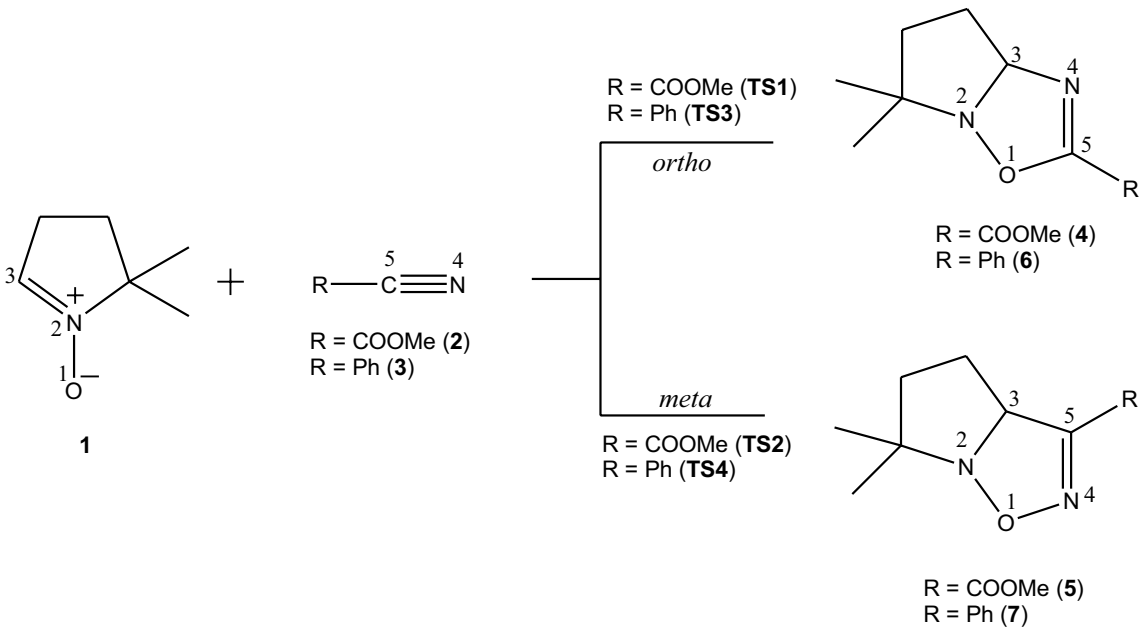

Scheme 3 Studied regioisomeric reaction paths of 32CA reactions of nitrone **1**, with nitriles **2** and **3**

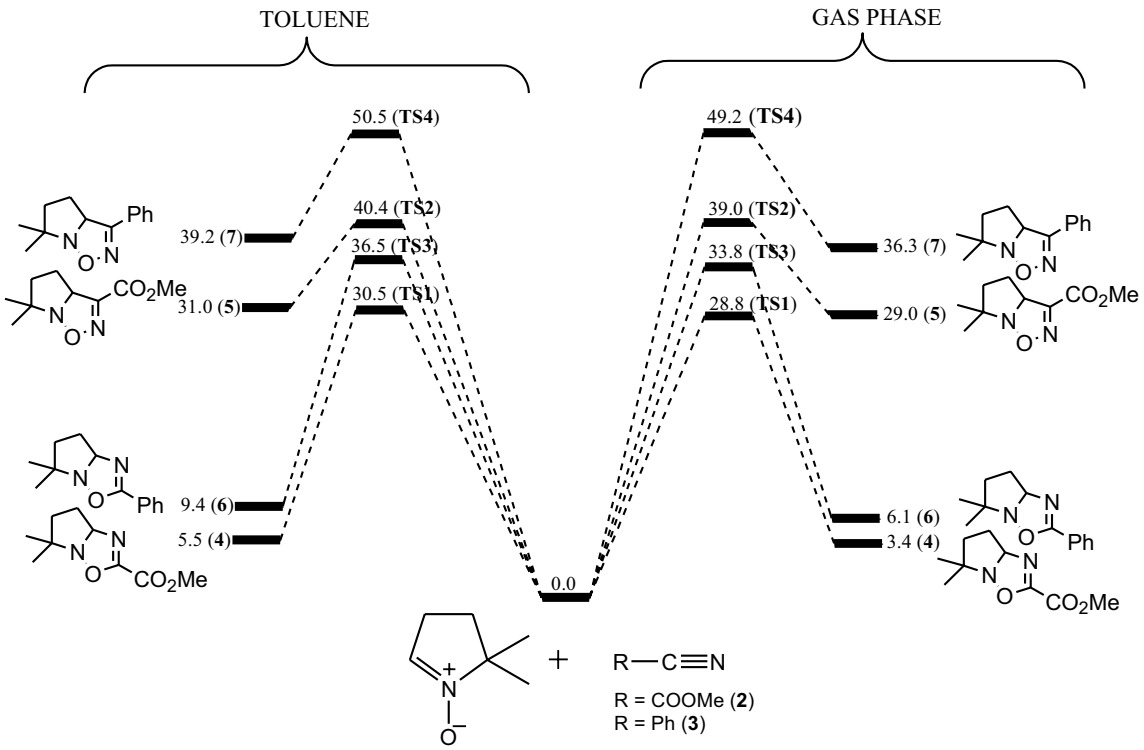

Scheme 4 Relative free energies (ΔG) in kcal·mol^{-1} of stationary points associated with the 32CA reactions of nitrone **1**, with nitriles **2** and **3** in gas phase and toluene

[5, 6]. (2) These 32CA reactions show activation free energies between 28.8 (**TS1**) and 49.2 (**TS4**) in gas phase and between 30.5 (**TS1**) and 50.5 (**TS4**) in toluene, in coherence with their *zw*-type classification associated with high activation parameters. (3) the inclusion of toluene increases the activation free energies by 1.3-2.7 kcal·mol^{-1} due to better solvation of the reagents than the TSs, while the reaction free energies are increased by 2.0–3.3 kcal·mol^{-1} in toluene [60] (3) the activation enthalpy for 32CA reaction of nitrone **1** with **2** via **TS1** is lowered by that for the 32CA reaction of nitrone **1** with **3** via **TS3** by 4.8 kcal·mol^{-1} in gas phase and by 6.0 kcal·mol^{-1} in toluene. The reaction enthalpy of the *ortho* adduct **4** obtained from the 32CA reaction of nitrone **1** with **2** is stabilized by 2 kcal·mol^{-1} in gas phase and by 3.6 kcal·mol^{-1} in toluene relative to the *ortho* adduct **6** obtained from the 32CA reaction of nitrone **1** with **3,** in agreement with the experimental studies, showing slower 32CA reactions with nitrile **3** relative to that with **2**.

Thermal corrections to the electronic energies give the relative enthalpies in gas phase and toluene. The activation enthalpies increase by 0.5–0.9 kcal·mol^{-1} in gas phase and by 0.4–0.8 kcal·mol^{-1} in toluene relative to the activation energies, while reaction enthalpies decrease by 1.9–2.5 kcal·mol^{-1} in gas phase and toluene relative to the reaction energies. Inclusion of the entropies to enthalpies strongly increases the activation Gibbs energies by 13.3–13.6 kcal·mol^{-1} in gas phase and toluene, while the reaction Gibbs energies show decrease by 13.9–14.6 kcal·mol^{-1} in gas phase and 14.1–14.4 kcal·mol^{-1} in toluene. The activation Gibbs free energy of **4** becomes 28.8 kcal·mol^{-1} in gas phase and 30.5 kcal·mol^{-1} in toluene, the 32CA reaction of **1** with **2** being endergonic by 3.4 kcal·mol^{-1} in gas phase and 5.5 kcal·mol^{-1} in toluene.

The B3LYP/6-311 ++G(d,p) optimised geometries of the TSs are given in Fig. 3. In gas phase, the distances between O1 and C5, and C3 and N4 interacting centres at the *ortho* TSs are: 1.803 and 2.011 Å, at **TS1** and 1.864 and 2.006 Å, at **TS3**, while the distances between O1 and N5, and C3 and C4 interacting centres at the *meta* TSs are: 2.135 and 1.744 Å, at **TS2** and 2.136 and 1.784 Å, at **TS4**, respectively. The TSs geometries show similar trend and minimal changes on inclusion of solvent effects in toluene. These geometrical parameters imply the extent of bond formation. (1) Considering that the C–O and C-N bond formation begins at the distances of 1.70–1.79 and 1.90–1.80 Å, respectively, these geometrical parameters indicate that at the *ortho* TSs **TS1** and **TS3**, the formation of the C–O or C–N single bonds has not yet begun [10]. (2) Considering that the C–C bond formation begins at the distances of 1.90 Å, it is evident that at the *meta* TSs **TS2** and **TS4**, the formation of the C–C single covalent bond has already started; however, the formation of

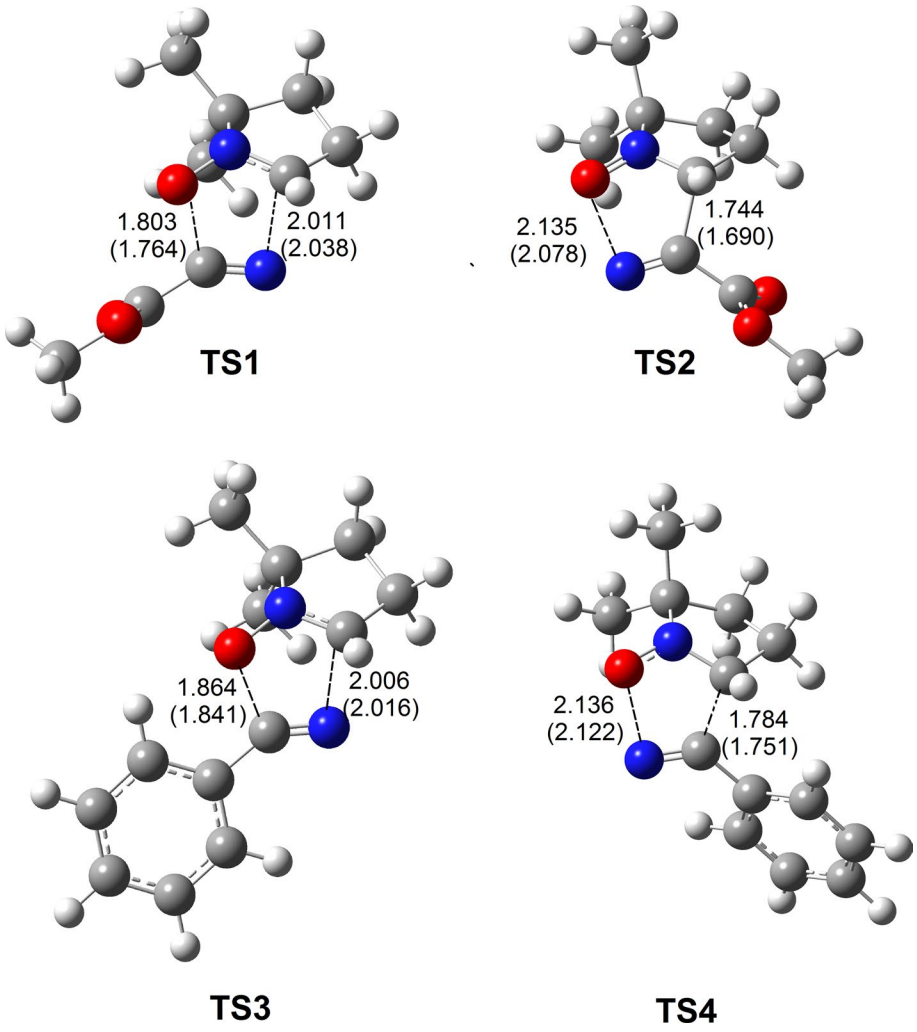

Fig. 3 B3LYP/6-311++G(d,p) optimised geometries of TSs involved in the 32CA reactions of nitrone **1** with nitriles **2** and **3.** Bond lengths are given in Angstroms. The values in parenthesis are calculated in toluene

N–O bond has not yet begun, owing to the O1–N5 distance being greater than 2.00 Å.

Finally, the polar nature of these 32CA reactions was evaluated by the GEDT calculations at the TSs [25]. The gas phase GEDT values at the TSs are 0.11 e at **TS1**, 0.17 e at **TS2**, 0.06 e at **TS3**, and 0.14 e at **TS4**. In toluene, the GEDT values at the TSs are 0.13 e at **TS1**, 0.17 e at **TS2**, 0.07 e at **TS3**, and 0.14 e at **TS4**. The electron density fluxes from nitrone **1** acting as the nucleophile towards nitriles **2** and **3** in each case, these reactions are classified as forward electron density flux (FEDF), evidenced by the higher nucleophilicity of nitrone **1** relative to the strongly electrophilic nitriles **2** and **3** (see Table 2) [61]. The higher GEDT values associated with the 32CA reaction of nitrone **1** with **2** relative to that with **3** accounts for the higher polar character and lower activation energy of the 32CA reaction with **2**. Note that, the unfavourable *meta* TSs with higher activation energies leading to less stable cycloadducts show higher GEDT values compared to the *ortho* TSs, owing to the dependence of the GEDT on three factors—the nucleophilicity and the electrophilicity of the reagents, and the distance between the two frameworks, the more unfavourable regioisomeric *meta* TS is more energetic and more advanced, which makes the GEDT higher at these TSs [25, 62].

3.4 Mechanistic implications along the regioisomeric channels of 32CA reaction of nitrone 1 with nitrile 2 from bonding evolution theory (BET) study

The bonding evolution theory (BET), proposed by Krokoidis, provides mechanistic implications along a reaction path by exploring the sequential bonding changes from the conjunction of the ELF topological analysis and Thoms catastrophe theory [20, 21, 26, 27]. For the 32CA reaction of nitrone **1** with nitrile **2**, the bonding pattern along the *ortho* and *meta* regioisomeric paths has been established from detailed BET study.

The ELF basin populations at the reacting centres for the 32CA reaction of nitrone **1** with nitrile **2** along the *ortho*

regioisomeric path and the proposed sequential bonding changes are given in Scheme 5. The identification of catastrophe from ELF basin analysis allows characterising six topological *phases I, II, III, IV, V* and *VI*, identified by the starting points **P1-I**, **P2-I**, **P3-I**, **P4-I**, **P5-I** and **P6-I**, respectively (Scheme 5).

The ELF topology of the starting point **P1-I** shows similar bonding pattern as the individual reagents (see Table 1). At **P2-I**, (d(C3–N4) = 2.222 Å, d(O1–C5) = 2.050 Å)), the monosynaptic basin V(N2) associated with the N2 nitrogen lone pair integrating 0.19 e is created by deriving electron density from the C3–N2 bonding region experiencing depopulation from 3.81 e at **P1-I** to 3.06 e at **P2-I**. Phases *III* and *IV* are, respectively, characterised by the creation of *pseudoradical* centres at C3 and C5, respectively, at **P3-I** and **P4-I** showing formation of monosynaptic basins V(C5) and V(C3) integrating 0.17 e and 0.21 e. Note that C5–N1 bonding region experiences depopulation from 3.96 e at **P3-I** to 3.79 e at **P4-I**, while the C3–N2 bonding region experiences depopulation from 2.66 e at **P3-I** to 2.37 e at **P4-I**. The transition structure **TS1** belongs to phase *III*. The energy cost (EC) for formation of *pseudoradical* centres at C5 and

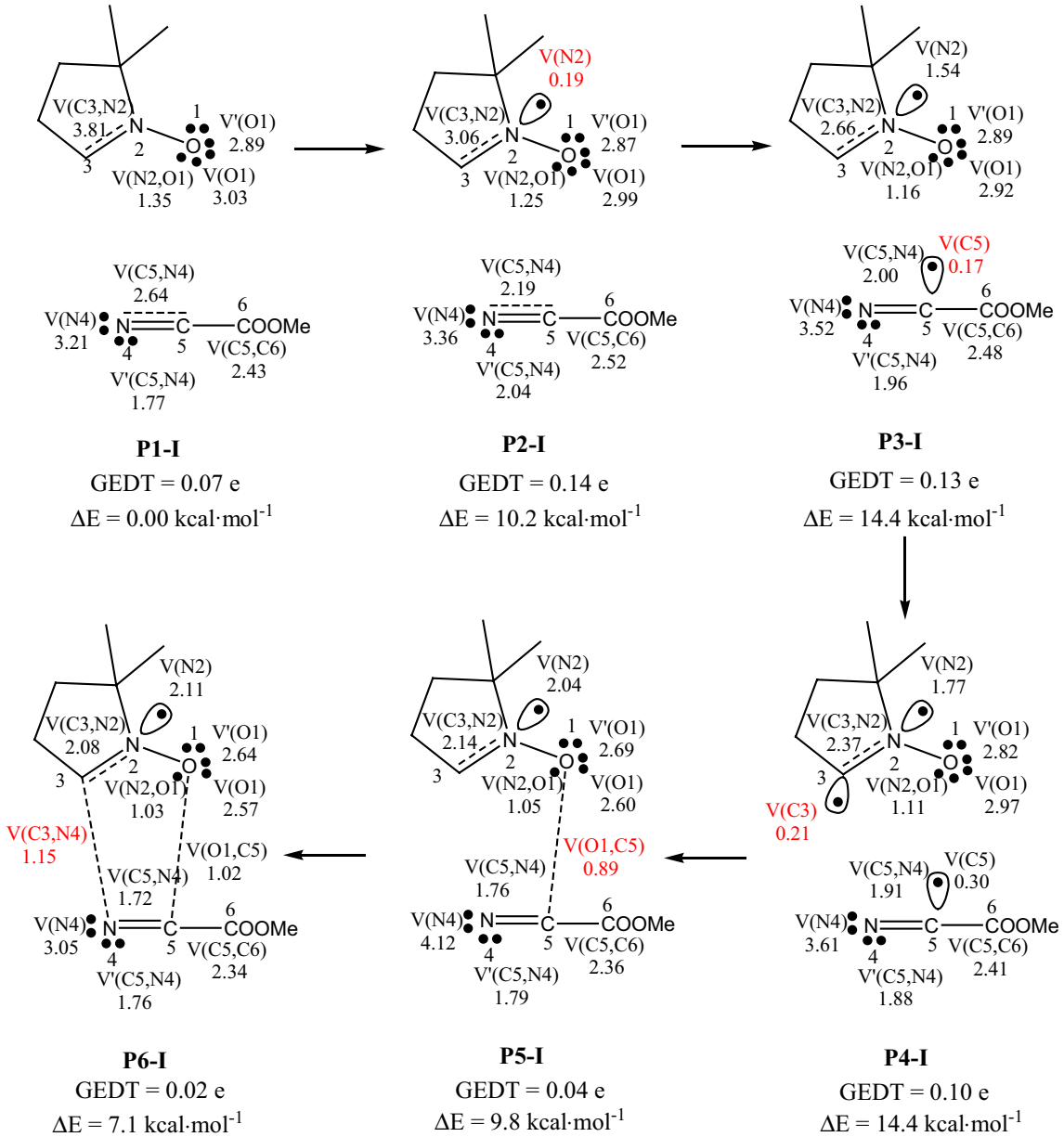

Scheme 5 Sequential bonding changes and most significant valence basin populations in average number of electrons e at the representative IRC points along the *ortho* reaction path of the 32 CA reaction of nitrone **1** with nitrile **2**

C3 and the lone pair electron density at N2 nitrogen corresponds to 98.6% of the activation energy. Note that at the TS, the formation of O1–C5 and C3–N4 covalent bonds has not begun, which agrees with the topological analysis of the AIM discussed in Sect. 3.6. In phase *V*, identified by the IRC point **P5-I**, the first O1–C5 single bond formation begins at the O1–C5 distance of 1.607 Å, characterised by the creation of disynaptic basin V(O1, C5) integrating 0.89 e, while in phase *VI*, identified by the IRC point **P6-I**, the second C3–N4 single bond formation begins at the C3–N4 distance of 1.793 Å, characterised by the creation of disynaptic basin V(C3,N4) integrating 1.15 e. Finally, at the cycloadduct **4**, the molecular geometry is relaxed at O1–C5 and C3–N4 distances of 1.361 and 1.463 Å, respectively.

The ELF basin populations at the reacting centres for the 32CA reaction of nitrone **1** with nitrile **2** along the *meta* regioisomeric path, and the sequential bonding changes are represented in Scheme 6. The identification of catastrophe from ELF basin analysis allows characterising seven topological *phases I, II, III, IV, V, VI* and *VII*, identified by the starting points **P1-II**, **P2-II**, **P3-II**, **P4-II**, **P5-II, P6-II** and **P7-II**, respectively (Scheme 6).

The ELF topology of the starting point **P1-II** shows similar bonding pattern as the individual reagents (see Table 1). At **P2-II**, (d(C3–C5) = 2.256 Å, d(O1–N4) = 2.388 Å)), the monosynaptic basin V(C3) integrating 0.31 e is created by deriving electron density from the C3–N2 bonding region, which shows depopulation from 3.83 e at **P1-II** to 3.46 e at **P2-II**. Phases *III* and *IV* are, respectively, characterised by the creation of *pseudoradical* centres at C5 and lone pair at N2 nitrogen, respectively, at **P3-II** and **P4-II** showing formation of monosynaptic basins V(C5) and V(N2) integrating 0.50 e and 0.71 e. Note that C5–N4 bonding region is depopulated from 4.19 e at **P2-II** to 3.96 e at **P3-II**, while the C3–N2 bonding region experiences depopulation from 3.43 e at **P3-II** to 2.71 e at **P4-II**.

In phase *V*, identified by the IRC point **P5-II**, the first C3-C5 single bond formation begins at the C3-C5 distance of 1.788 Å, characterised by the creation of disynaptic basin V(C3,C5) integrating 1.55 e. The energy cost (EC) for the creation of lone pair electron density at N2 nitrogen and formation of C3–C5 single bond corresponds to 100% of the activation energy. The transition structure **TS2** belongs to phase *V*. Note that at the TS, the formation of C3–C5 covalent bond has begun, also indicated by the negative Laplacian of electron density in the AIM topological analysis discussed in Sect. 3.6. In phase *VI*, identified by the IRC point **P6-II**, there is creation of monosynaptic basins V'''(O1) and V'(N4), integrating at 0.23 e and 0.27 e, respectively, associated with the lone pair electron density at the O1 oxygen and N4 nitrogen. Finally, in phase *VII*, **at P7-II**, the second O1–N4 single bond formation begins at the O1–N4 distance of 1.484 Å, characterised by the creation of disynaptic basin V(O1,N4) integrating 0.97 e. The molecular geometry is finally relaxed at C3–C5 and O1–N4 distances of 1.514 and 1.475 Å, respectively, in the cycloadduct **5**. Note that the formation of the second O1–N4 begins when the total integrating population of disynaptic basin V(C3,C5) has reached 2.01 e. Thus, the *one-step two-stage* mechanism is predicted for the *meta* reaction path.

A comparative analysis of the BET of the *ortho* and *meta* reaction paths for 32CA reaction of nitrone **1** with nitrile **2** allows arriving at some important conclusions (1) Along the *ortho* reaction path, the lone pair electron density is created at N2 nitrogen in the first phase, while in the *meta* reaction path, the *pseudoradical* centres at C3 and C5 demanded for the formation of the new C3–C5 bond are created in the first two phases. The total integrating population of V(C5) and V(C3) basins at the starting points are 0.21 e and 0.17 e, while the respective populations along the *meta* reaction paths are 0.31 e and 0.50 e. These observations predict more advanced C3–C5 bond formation at the *meta* reaction path, consequently leading to increase in GEDT at **P2-II** (0.15 e) and **P3-II** (0.18 e) associated with the *meta* reaction path compared to **P3-I** (0.13 e) and **P4-I** (0.10 e) associated with the *ortho* reaction path. (2) At the *ortho* **TS1**, the formation of no new covalent single bond has begun, while at the *meta* **TS2** shows formation of new C3–C5 single bond. (3) Although the *meta* reaction path is more advanced relative to the *ortho* reaction path, the EC demanded at IRC points **P2-II**, **P3-II** and **P4-II** associated with the *meta* reaction path are higher than that demanded by the IRC points **P2-I**, **P3-I** and **P4-I** associated with the *ortho* reaction path by 6.9, 6.9 and 8.1 kcal·mol^{-1}, resulting in the increased activation energy barrier of **TS2** relative to **TS1** by 10.4 kcal·mol^{-1}. (4) These 32CA reactions show positive relative Gibbs free energies, suggesting endergonic character, and hence the decisive role of the relative energies of the cycloadducts in the product composition. Along the *ortho* and *meta* reaction channels, the BET studies suggest relaxation of the molecular geometries in phase *VII* at the cycloadducts **4** and **5** with relative energies − 13.0 and 12.6 kcal·mol^{-1}, which clearly indicates the preferred formation of *ortho* adduct **4**, in agreement with the experimental outcome.

3.5 ELF topological analysis at the TSs

The ELF valence basin populations at the four TSs, **TS1**, **TS2**, **TS3** and **TS4** are listed in Table 3, while the ELF localisation domains are represented in Fig. 4. ELF of the *ortho* TSs, **TS1** and **TS3** show the presence of monosynaptic V(N2) and V(C5) basins integrating 1.66 e and 0.23–0.24 e, which are absent in the ELF of nitrone **1**. The disynaptic V(C3,N2) basin in nitrone **1** associated with the C3-N2 bonding region integrating 3.84 e in nitrone **1** is depopulated to 2.62 e in **TS1**, 2.11 e in **TS2**, 2.62 e in **TS3** and 2.17 e in

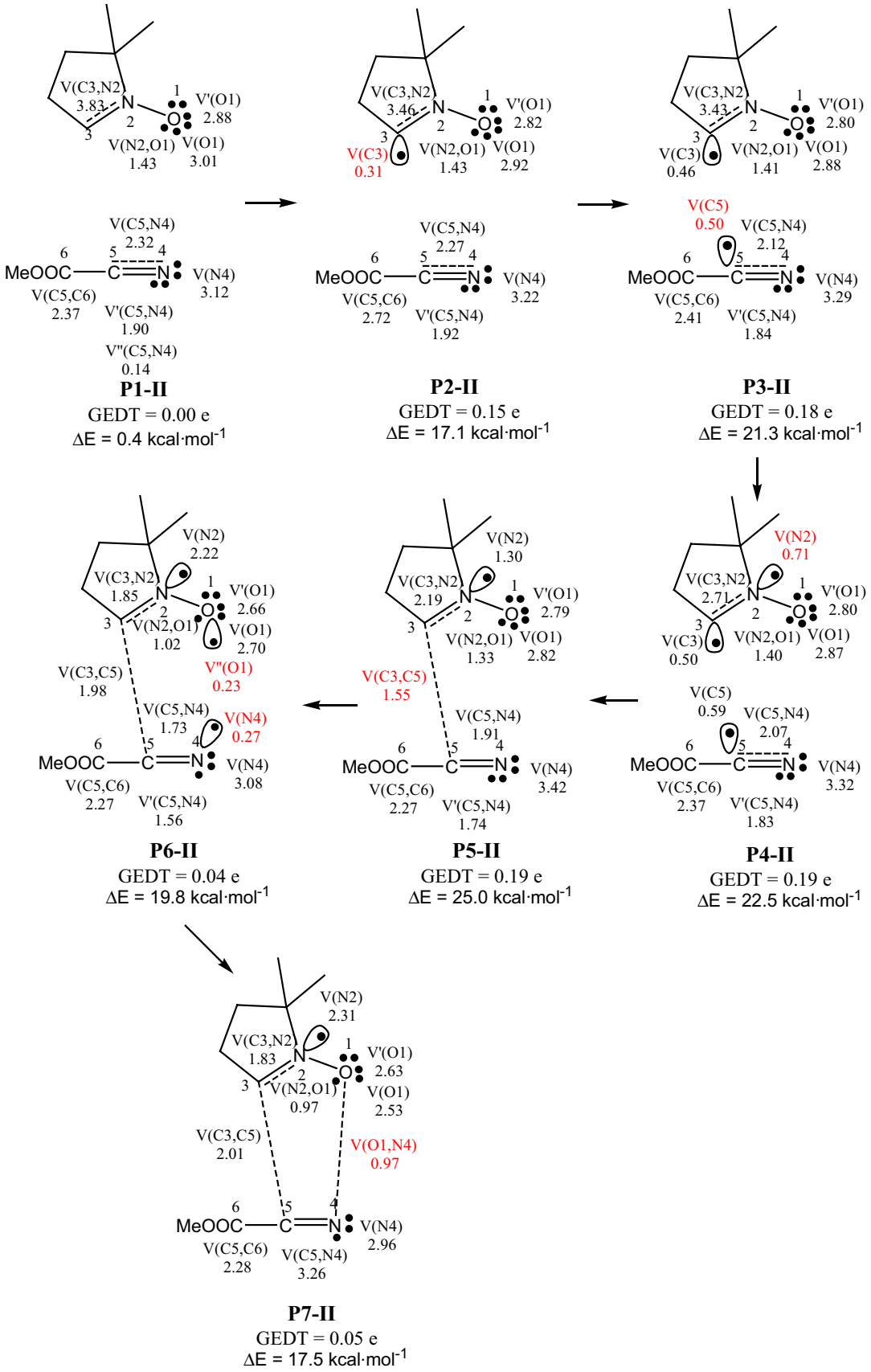
V(C3,N2) 3.83
V'(O1) 2.88
V(N2,O1) 1.43
V(O1) 3.01
V(C3,N2) 3.46
V'(O1) 2.82
V(C3) 0.31
V(N2,O1) 1.43
V(O1) 2.92
V(C3,N2) 3.43
V'(O1) 2.80
V(C3) 0.46
V(N2,O1) 1.41
V(O1) 2.88
V(C5,N4) 2.32
MeOOC
V(N4) 3.12
V(C5,C6) 2.37
V'(C5,N4) 1.90
V''(C5,N4) 0.14
V(C5,N4) 2.27
V(N4) 3.22
V(C5,C6) 2.72
V'(C5,N4) 1.92
V(C5) 0.50
V(C5,N4) 2.12
V(N4) 3.29
V(C5,C6) 2.41
V'(C5,N4) 1.84
P1-II
GEDT = 0.00 e
ΔE = 0.4 kcal·mol-1
P2-II
GEDT = 0.15 e
ΔE = 17.1 kcal·mol-1
P3-II
GEDT = 0.18 e
ΔE = 21.3 kcal·mol-1
V(N2) 2.22
V(C3,N2) 1.85
V'(O1) 2.66
V(N2,O1) 1.02
V(O1) 2.70
V''(O1) 0.23
V(C3,C5) 1.98
V(C5,N4) 1.73
V(N4) 0.27
V(N4) 3.08
V(C5,C6) 2.27
V'(C5,N4) 1.56
V(N2) 1.30
V(C3,N2) 2.19
V'(O1) 2.79
V(N2,O1) 1.33
V(O1) 2.82
V(C3,C5) 1.55
V(C5,N4) 1.91
V(N4) 3.42
V(C5,C6) 2.27
V'(C5,N4) 1.74
V(N2) 0.71
V(C3,N2) 2.71
V'(O1) 2.80
V(C3) 0.50
V(N2,O1) 1.40
V(O1) 2.87
V(C5) 0.59
V(C5,N4) 2.07
V(N4) 3.32
V(C5,C6) 2.37
V'(C5,N4) 1.83
P6-II
GEDT = 0.04 e
ΔE = 19.8 kcal·mol-1
P5-II
GEDT = 0.19 e
ΔE = 25.0 kcal·mol-1
P4-II
GEDT = 0.19 e
ΔE = 22.5 kcal·mol-1
V(N2) 2.31
V(C3,N2) 1.83
V'(O1) 2.63
V(N2,O1) 0.97
V(O1) 2.53
V(C3,C5) 2.01
V(O1,N4) 0.97
V(N4) 2.96
V(C5,C6) 2.28
V(C5,N4) 3.26
P7-II
GEDT = 0.05 e
ΔE = 17.5 kcal·mol-1

◂**Scheme 6** Sequential bonding changes and most significant valence basin populations in average number of electrons e at the representative IRC points along the *meta* reaction path of the 32 CA reaction of nitrone **1** with nitrile **2**

Table 3 B3LYP/6-311 ++G(d,p) calculated ELF valence basin populations at the TSs

	TS1	TS2	TS3	TS4
V(O1)	2.94	2.78	2.90	2.78
V'(O1)	2.86	2.82	2.96	2.83
V(N2)	1.66	1.41	1.66	1.41
V(C3,N2)	2.62	2.11	2.62	2.17
V(N2,O1)	1.14	1.31	1.14	1.31
V(N4)	3.57	3.43	3.60	3.46
V(N4,C5)	1.95	1.72	1.95	1.73
V'(N4,C5)	1.92	1.87	1.85	1.84
V(C5,C6)	2.44	2.26	2.43	2.19
V(C5)	0.24		0.23	
V(C3,C5)		1.62		1.59

TS4. The disynaptic V(N4,C5) basin in the nitriles associated with the N4–C5 bonding region integrating 4.50 e (**2**) and 4.40 e (**3**) in the nitriles is depopulated to 3.87 e in **TS1**, 3.59 e in **TS2**, 3.80 e in **TS3** and 3.57 e in **TS4**. At the *ortho* TSs, the formation of new single covalent bond has not been started, while at the *meta* TSs, the presence of disynaptic basin V(C3,C5) integrating 1.62 e (**TS2**) and 1.59 e (**TS4**) suggests that the formation of C3–C5 single bond has been started at **TS2** and **TS4**.

3.6 QTAIM topological analysis at TSs

The nature of interactions at the interatomic reacting centres of the TSs was evaluated from the topological analysis of the AIM proposed by Bader and coworkers [28, 29]. The bond critical points **CP1**, for the newly formed O1–C5 (**TS1, TS3**) and O1–N4 (**TS2, TS4**) bonds, and **CP2**, for the newly formed C3–N4 (**TS1, TS3**) and C3–C5 (**TS2, TS4**) bonds are represented in Scheme 7, while the electron density ρ, the Laplacian of electron density, $\nabla^2_{\rho(r_c)}$ and the energy density $E_{\rho(r_c)}$ at **CP1** and **CP2** are given in Table 4. At the *ortho* and *meta* TSs, **CP1** shows positive Laplacian of electron density and low electron density, suggesting that the formation of O1–C5 or O1–N4 covalent bonds has not been started at the TSs, the observation being in conformity with the ELF study showing absence of disynaptic basins V(O1,C5) or V(O1,N4) at the TSs (Sect. 3.5). At the *ortho* TSs, **TS1** and **TS3**, **CP2** shows positive Laplacian of electron density and low electron density, suggesting that the formation of C3–N4 covalent bonds has not been started at these TSs. However, **CP2** corresponding to the formation of new C3–C5 single bonds at the *meta* TSs **TS2** and **TS4** shows negative Laplacian of electron density and value of calculated electron density $\rho > 0.1$ au, which indicates covalent bonding between C3 and C5, in complete agreement with the ELF study showing the presence of disynaptic basins V(C3,C5) at these TSs (Sect. 3.5).

4 Conclusion

An MEDT study is presented for 32CA reaction of a 2,2-dimethyl-1-pyrroline-1-oxide **1** to nitriles **2** and **3** at the B3LYP/6-311 ++G(d,p) computational level.

The ELF topological analysis at the ground state structures allows classification of the nitrone **1** as a zwitterionic TAC, allowing its participation in *zw*-type 32CA reactions, demanding appropriate electrophilic–nucleophilic interactions. Nitriles **2** and **3** show underpopulated C≡N bonding region.

The global electronic flux from the nitrone **1** to nitrile **2** and **3** is predicted, owing to the high electronic chemical potential and strong nucleophilicity of the cyclic nitrone **1** relative to the nitriles **2** and **3**, which is confirmed from the GEDT calculations at the located TSs. Nitrile **2** shows lower electronic chemical potential and higher electrophilicity relative to nitrile **3**, suggesting a more facile reaction with nitrone **1**, also suggested by the higher GEDT for the 32CA reaction of nitrone **1** with nitrile **2**, relative to that with **3**.

These 32CA reactions are endergonic with positive free energy of reaction. The 2,3-dihydro-1,2,4-oxadiazole derivatives show higher thermodynamic stability relative to the 2,3-dihydro-1,2,5-oxadiazole derivatives, suggesting regioselectivity in complete coherence with the experiments. The 2,3-dihydro-1,2,4-oxadiazole obtained from the 32CA reaction of nitrone **1** with nitrile **2** is thermodynamically more stable compared to that generated from the 32CA reaction of with nitrile **3**.

BET study along the regioisomeric reaction channels allows arriving at some important mechanistic conclusions. Along both the reaction paths, in the first four *phases*, the C=N bonding region of nitrone **1** and C≡N bonding region of the nitrile **2** are depopulated to create *pseudoradical* centres at C5 and C3 carbons and lone pair electron density at N2 nitrogen. The 32CA reaction of *meta* reaction path is more advanced relative to the *ortho* reaction path, indicated by the higher basin populations of monosynaptic basins V(C5), V(C3) and V(N2), accounting for the higher GEDT at the IRC points and at the TSs. The *ortho* reaction path follows *one-step* mechanism, and

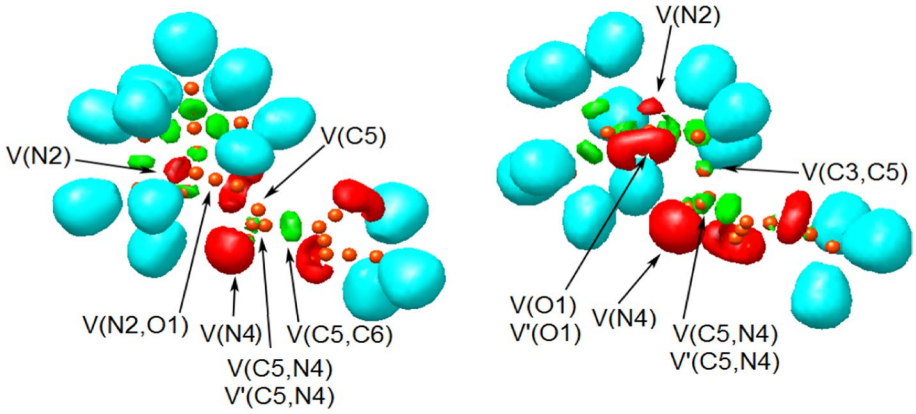

Fig. 4 B3LYP/6-311++G(d,p) ELF localisation domains represented at an isosurface value of ELF = 0.83 of **TS1** and **TS2.** Blue colour represents the protonated basins, green coloured ones are the disynaptic basins, and red colour is used to represent the monosynaptic basins. The attractor positions are represented as orange spheres

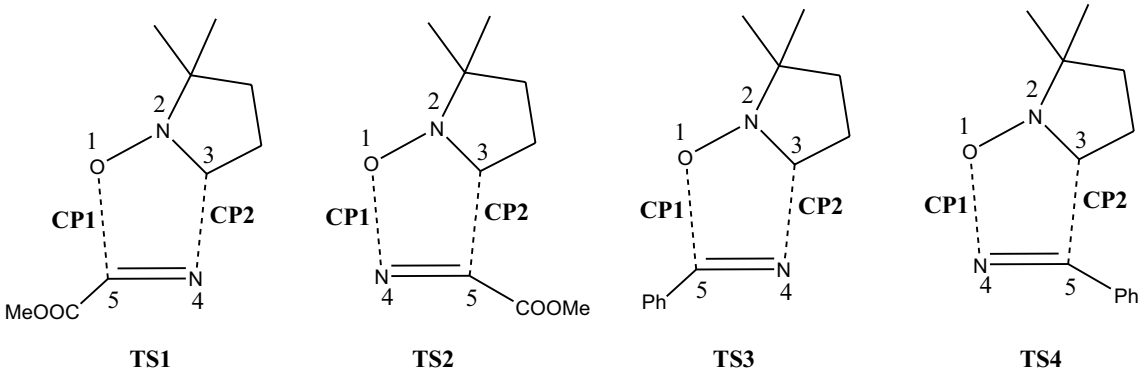

Scheme 7 Bond critical points **CP1** and **CP2** at the TSs in the regions associated with formation of new single bonds

Table 4 QTAIM parameters, in au, of (3,-1) CPs at the TSs in the regions associated with formation of new O1-C5 (**CP1 (TS1, TS3)**), O1-N4 (**CP1 (TS2, TS4)**), C3-N4 (**CP2 (TS1, TS3)**) and C3-C5 (**CP2 (TS2, TS4)**) single bonds

	CP1 (O1-C5/O1-N4)			**CP2** (C3-N4/C3-C5)		
	ρ	$\nabla^2_{\rho(r_c)}$	$E_{\rho(r_c)}$	ρ	$\nabla^2_{\rho(r_c)}$	$E_{\rho(r_c)}$
TS1	0.011	0.124	−0.037	0.078	0.087	−0.018
TS2	0.055	0.172	0.003	0.151	−0.137	−0.078
TS3	0.010	0.132	−0.025	0.079	0.089	−0.018
TS4	0.055	0.171	0.002	0.140	−0.107	−0.068

the formation of second C3–N4 single bond starts when 68% bond formation of the first O1–C5 single bond has been completed. The *meta* reaction path follows *one-step two-stage* mechanism and the formation of second O1–N4 single bond starts when the first C3–C5 bonding region has reached basin population of 2.01 e.

ELF study at the TSs and the calculated QTAIM parameters shows early TSs along the *ortho* reaction path, when the formation of new single covalent bond has not been started. On the other hand, the C3–C5 single bond has been formed at the *meta* TSs indicated by the negative Laplacian of electron density and formation of V(C3,C5) disynaptic basin.

Compliance with ethical standards

Conflict of interest The authors declare no conflict of interest.

References

1. Plate R, Hermkens PHH, Smits JMM, Nivard RJF, Ottenheijm HCJ (1987) Employment of nitriles in the stereoselective cycloaddition to nitrones. J Organ Chem 52(6):1047–1051. https://doi.org/10.1021/jo00382a014

2. Hermkens PHH, Maarseveen JHV, Kruse CG, Scheeren HW (1988) 1,3-Dipolar cycloaddition of nitrones with nitriles: scope and mechanistic study. Tetrahedron 44(20):6491–6504. https://doi.org/10.1016/S0040-4020(01)89838-0
3. Bokach NA, Kukushkin VY (2006) 1,3-dipolar cycloaddition of nitrones to free and coordinated nitriles: routes to control the synthesis of 2,3-dihydro-1,2,4-oxadiazoles. Russ Chem Bull 55(11):1869–1882. https://doi.org/10.1007/s11172-006-0528-0
4. Bokach NA, Kuznetsov ML, Kukushkin VY (2011) 1,3-Dipolar cycloaddition of nitrone-type dipoles to uncomplexed and metal-bound substrates bearing the CN triple bond. Coord Chem Rev 255(23):2946–2967. https://doi.org/10.1016/j.ccr.2011.07.001
5. Yu Y, Watanabe N, Ohno M, Eguchi S (1995) Synthesis of novel carbo- and heteropolycycles. Part 30. 1,3-Dipolar cycloaddition of nitrile functions with some selected nitrones. Efficient synthesis of 2,3-dihydro-1,2,4-oxadiazole derivatives. J Chem Soc Perkin Trans 1(11):1417–1421. https://doi.org/10.1039/P19950001417
6. Yu Y, Fujita H, Ohno M, Eguchi S (1995) 1,3-Dipolar cycloaddition of nitrile functions with nitrones under high pressure conditions. A new and direct synthesis of 2,3-Dihydro-1,2,4-Oxadiazole derivatives. Synthesis 05:498–500. https://doi.org/10.1055/s-1995-3949
7. Yu Y, Ohno M, Eguchi S (1994) Remarkable dipolarophilicity of nitrile function uncovered in the 1,3-dipolar cycloaddition reaction of homoadamantane-incorporated nitrones. A direct and facile route to Δ4-1,2,4-oxadiazoline (2,3-dihydro-1,2,4-oxadiazole) derivatives. J Chem Soc Chem Commun 3:331–332. https://doi.org/10.1039/C39940000331
8. Krylov A, Windus TL, Barnes T, Marin-Rimoldi E, Nash JA, Pritchard B, Smith DGA, Altarawy D, Saxe P, Clementi C, Crawford TD, Harrison RJ, Jha S, Pande VS, Head-Gordon T (2018) Perspective: computational chemistry software and its advancement as illustrated through three grand challenge cases for molecular science. J Chem Phys 149(18):180901. https://doi.org/10.1063/1.5052551
9. Domingo LR (2016) Molecular electron density theory: a modern view of reactivity in organic chemistry. Molecules 21(10):1319. https://doi.org/10.3390/molecules21101319
10. Ríos-Gutiérrez M, Domingo LR (2019) Unravelling the mysteries of the [3 + 2] cycloaddition reactions. Eur J Org Chem 2–3:267–282. https://doi.org/10.1002/ejoc.201800916
11. Domingo LR, Ríos-Gutiérrez M, Pérez P (2018) A molecular electron density theory study of the reactivity and selectivities in [3 + 2] cycloaddition reactions of C, N-dialkyl nitrones with ethylene derivatives. J Organ Chem 83(4):2182–2197. https://doi.org/10.1021/acs.joc.7b03093
12. Mohammad-Salim H, Hassan R, Abdallah HH, Oftadeh M (2020) The theoretical study on the mechanism of [3 + 2] cycloaddition reactions between α, β-unsaturated selenoaldehyde with nitrone and with nitrile oxide. J Mex Chem Soc. https://doi.org/10.29356/jmcs.v64i2.1111
13. Domingo LR, Acharjee N (2020) Unravelling the strain-promoted [3 + 2] cycloaddition reactions of phenyl azide with cycloalkynes from the molecular electron density theory perspective. New J Chem 44(32):13633–13643. https://doi.org/10.1039/D0NJ02711A
14. Domingo LR, Acharjee N (2020) Unveiling the high reactivity of strained dibenzocyclooctyne in [3 + 2] cycloaddition reactions with diazoalkanes through the molecular electron density theory. J Phys Org Chem. https://doi.org/10.1002/poc.4100
15. Domingo LR, Acharjee N (2020) A molecular electron density theory study of the Grignard reagent-mediated regioselective direct synthesis of 1,5-disubstituted-1,2,3-triazoles. J Phys Org Chem 33(8):e4062. https://doi.org/10.1002/poc.4062
16. Domingo LR, Ríos-Gutiérrez M, Acharjee N (2019) A molecular electron density theory study of the chemoselectivity, regioselectivity, and diastereofacial selectivity in the synthesis of an anticancer spiroisoxazoline derived from α-santonin. Molecules 24(5):832. https://doi.org/10.3390/molecules24050832
17. Abbiche K, Mohammad-Salim H, Salah M, Mazoir N, Zeroual A, El Abdallaoui HEA, El Hammadi A, Hilali M, Abdallah HH, Hochlaf M (2020) Insights into the mechanism and regiochemistry of the 1,3-dipolar cycloaddition reaction between benzaldehyde and diazomethane. Theoret Chem Acc 139(9):148. https://doi.org/10.1007/s00214-020-02662-4
18. Wagner G (2003) Theoretical study of the [2 + 3] cycloaddition of nitrones to nitriles—influence of nitrile substituent, solvent and lewis acid coordination. Chem A Eur J 9(7):1503–1510. https://doi.org/10.1002/chem.200390172
19. Kuznetsov ML, Kukushkin VY, Dementev AI, Pombeiro AJL (2003) 1,3-dipolar cycloaddition of nitrones to free and Pt-bound nitriles. A theoretical study of the activation effect, reactivity, and mechanism. J Phys Chem A 107(31):6108–6120. https://doi.org/10.1021/jp035261k
20. Becke AD, Edgecombe KE (1990) A simple measure of electron localization in atomic and molecular systems. J Chem Phys 92(9):5397–5403. https://doi.org/10.1063/1.458517
21. Silvi B, Savin A (1994) Classification of chemical bonds based on topological analysis of electron localization functions. Nature 371(6499):683–686. https://doi.org/10.1038/371683a0
22. Geerlings P, De Proft F, Langenaeker W (2003) Conceptual density functional theory. Chem Rev 103(5):1793–1874. https://doi.org/10.1021/cr990029p
23. Domingo LR, Ríos-Gutiérrez M, Pérez P (2016) Applications of the conceptual density functional theory indices to organic chemistry reactivity. Molecules 21(6):748
24. Sutcliffe BT (2006) The idea of a potential energy surface. Mol Phys 104(5–7):715–722. https://doi.org/10.1080/00268970500418059
25. Domingo LR (2014) A new C-C bond formation model based on the quantum chemical topology of electron density. RSC Adv 4(61):32415–32428. https://doi.org/10.1039/C4RA04280H
26. Thom R (1974) Stabilité Structurelle et Morphogenèse (Interéditions) 1972. THOM, R, Modèles Mathématiques de la Morphogenèse (Edi-tions 10-18)
27. Krokidis X, Silvi B, Alikhani ME (1998) Topological characterization of the isomerization mechanisms in XNO (X = H, Cl). Chem Phys Lett 292(1):35–45. https://doi.org/10.1016/S0009-2614(98)00650-2
28. Bader RFW, Bader RF (1990) Atoms in molecules: a quantum theory. Clarendon Press, Oxford
29. Bader RF, Essén H (1984) The characterization of atomic interactions. J Chem Phys 80(5):1943–1960
30. Schlegel HB (1982) Optimization of equilibrium geometries and transition structures. J Comput Chem 3(2):214–218. https://doi.org/10.1002/jcc.540030212
31. Wiberg KB (1986) Ab initio molecular orbital theory by W. J. Hehre, L. Radom, P. v. R. Schleyer, and J. A. Pople, John Wiley, New York, 548 pp. J Comput Chem 7(3):379–379. https://doi.org/10.1002/jcc.540070314
32. Mohammad-Salim HA, Acharjee N, Domingo LR, Hassan HH (2020) A molecular electron density theory study for [3 + 2] cycloaddition reactions of 1-Pyrroline-1-oxide with disubstituted acetylenes leading to bicyclic 4-isoxazolines. Int J Quantum Chem. https://doi.org/10.1002/qua.26503
33. Dresler E, Kącka-Zych A, Kwiatkowska M, Jasiński R (2018) Regioselectivity, stereoselectivity, and molecular mechanism of [3 + 2] cycloaddition reactions between 2-methyl-1-nitroprop-1-ene and (Z)-C-aryl-N-phenylnitrones: a DFT computational study. J Mol Model 24(11):329. https://doi.org/10.1007/s00894-018-3861-y

34. Alnajjar RA, Jasiński R (2019) Competition between [2 + 1]- and [4 + 1]-cycloaddition mechanisms in reactions of conjugated nitroalkenes with dichlorocarbene in the light of a DFT computational study. J Mol Model 25(6):157. https://doi.org/10.1007/s00894-019-4006-7
35. Adjieufack AI, Ndassa IM, Mbadcam JK, Ríos-Gutiérrez M, Domingo LR (2016) Understanding the reaction mechanism of the Lewis acid (MgBr 2)-catalysed [3 + 2] cycloaddition reaction between C-methoxycarbonyl nitrone and 2-propen-1-ol: a DFT study. Theoret Chem Acc 136(1):5. https://doi.org/10.1007/s00214-016-2028-0
36. Fukui K (1970) Formulation of the reaction coordinate. J Phys Chem 74(23):4161–4163. https://doi.org/10.1021/j100717a029
37. Gonzalez C, Schlegel HB (1990) Reaction path following in mass-weighted internal coordinates. J Phys Chem 94(14):5523–5527. https://doi.org/10.1021/j100377a021
38. Gonzalez C, Schlegel HB (1991) Improved algorithms for reaction path following: higher-order implicit algorithms. J Chem Phys 95(8):5853–5860. https://doi.org/10.1063/1.461606
39. Tomasi J, Persico M (1994) Molecular interactions in solution: an overview of methods based on continuous distributions of the solvent. Chem Rev 94(7):2027–2094. https://doi.org/10.1021/cr00031a013
40. Simkin BIAK, Sheĭkhet III (1995) Quantum chemical and statistical theory of solutions: a computational approach. Ellis Horwood, Chichester
41. Cossi M, Barone V, Cammi R, Tomasi J (1996) Ab initio study of solvated molecules: a new implementation of the polarizable continuum model. Chem Phys Lett 255(4):327–335. https://doi.org/10.1016/0009-2614(96)00349-1
42. Cancès E, Mennucci B, Tomasi J (1997) A new integral equation formalism for the polarizable continuum model: theoretical background and applications to isotropic and anisotropic dielectrics. J Chem Phys 107(8):3032–3041. https://doi.org/10.1063/1.474659
43. Barone V, Cossi M, Tomasi J (1998) Geometry optimization of molecular structures in solution by the polarizable continuum model. J Comput Chem 19(4):404–417. https://doi.org/10.1002/(sici)1096-987x(199803)19:4%3c404:aid-jcc3%3e3.0.co;2-w
44. Reed AE, Weinstock RB, Weinhold F (1985) Natural population analysis. J Chem Phys 83(2):735–746. https://doi.org/10.1063/1.449486
45. Reed AE, Curtiss LA, Weinhold F (1988) Intermolecular interactions from a natural bond orbital, donor-acceptor viewpoint. Chem Rev 88(6):899–926. https://doi.org/10.1021/cr00088a005
46. Lu T, Chen F (2012) Multiwfn: a multifunctional wavefunction analyzer. J Comput Chem 33(5):580–592. https://doi.org/10.1002/jcc.22885
47. Pettersen EF, Goddard TD, Huang CC, Couch GS, Greenblatt DM, Meng CC, Ferrin TE (2004) UCSF Chimera–a visualization system for exploratory research and analysis. J Comput Chem 25(13):12–1605. https://doi.org/10.1002/jcc.20084
48. Frisch M, Trucks G, Schlegel H, Scuseria G, Robb M, Cheeseman J, Scalmani G, Barone V, Petersson G, Nakatsuji H (2016) Gaussian 16. Gaussian, Inc., Wallingford
49. Huisgen R (1976) 1,3-Dipolar cycloadditions. 76. Concerted nature of 1,3-dipolar cycloadditions and the question of diradical intermediates. J Organ Chem 41(3):403–419. https://doi.org/10.1021/jo00865a001
50. Parr RG, Yang W (1995) Density-functional theory of the electronic structure of molecules. Annu Rev Phys Chem 46(1):701–728. https://doi.org/10.1146/annurev.pc.46.100195.003413
51. Domingo LR, Ríos-Gutiérrez M, Duque-Noreña M, Chamorro E, Pérez P (2016) Understanding the carbenoid-type reactivity of nitrile ylides in [3 + 2] cycloaddition reactions towards electron-deficient ethylenes: a molecular electron density theory study. Theoret Chem Acc 135(7):160. https://doi.org/10.1007/s00214-016-1909-6
52. Domingo LR, Acharjee N (2018) [3 + 2] cycloaddition reaction of C-Phenyl-N-methyl nitrone to acyclic-olefin-bearing electron-donating substituent: a molecular electron density theory study. ChemistrySelect 3(28):8373–8380. https://doi.org/10.1002/slct.201801528
53. Acharjee N, Banerji A (2020) A molecular electron density theory study to understand the interplay of theory and experiment in nitrone-enone cycloaddition. J Chem Sci 132(1):65. https://doi.org/10.1007/s12039-020-01766-5
54. Domingo LR, Aurell MJ, Pérez P, Contreras R (2002) Quantitative characterization of the global electrophilicity power of common diene/dienophile pairs in Diels-Alder reactions. Tetrahedron 58(22):4417–4423. https://doi.org/10.1016/S0040-4020(02)00410-6
55. Jaramillo P, Domingo LR, Chamorro E, Pérez P (2008) A further exploration of a nucleophilicity index based on the gas-phase ionization potentials. J Mol Struct (Thoechem) 865(1):68–72. https://doi.org/10.1016/j.theochem.2008.06.022
56. Parr RG, Weitao Y (1994) Density-functional theory of atoms and molecules. Oxford University Press, Oxford
57. Parr RG, Pearson RG (1983) Absolute hardness: companion parameter to absolute electronegativity. J Am Chem Soc 105(26):7512–7516. https://doi.org/10.1021/ja00364a005
58. Parr RG, Lv Szentpály, Liu S (1999) Electrophilicity index. J Am Chem Soc 121(9):1922–1924. https://doi.org/10.1021/ja983494x
59. Domingo LR, Chamorro E, Pérez P (2008) Understanding the reactivity of captodative ethylenes in polar cycloaddition reactions. A theoretical study. J Organ Chem 73(12):4615–4624. https://doi.org/10.1021/jo800572a
60. Benchouk W, Mekelleche SM, Silvi B, Aurell MJ, Domingo LR (2011) Understanding the kinetic solvent effects on the 1,3-dipolar cycloaddition of benzonitrile N-oxide: a DFT study. J Phys Org Chem 24(7):611–618. https://doi.org/10.1002/poc.1858
61. Domingo LR, Ríos-Gutiérrez M, Pérez P (2020) A molecular electron density theory study of the participation of tetrazines in aza-Diels–Alder reactions. RSC Adv 10(26):15394–15405. https://doi.org/10.1039/D0RA01548B
62. Domingo LR, Ríos-Gutiérrez M, Pérez P (2020) Unveiling the lewis acid catalyzed diels-alder reactions through the molecular electron density theory. Molecules 25(11):2535. https://doi.org/10.3390/molecules25112535